

Identification of a Parametrized Family of Chaotic Dynamics from Time Series

Isao Tokuda¹ and Ryuji Tokunaga²

¹ Department of Computer Science and Systems Engineering,
Muroran Institute of Technology, Muroran, Hokkaido, 050-8585, Japan
tokuda@csse.muroran-it.ac.jp

² Institute of Information Sciences and Electronics,
University of Tsukuba, Tsukuba Science City, Ibaraki 305, Japan
tokunaga@chaos.is.tsukuba.ac.jp

Abstract

In this chapter, we consider the problem of identifying an unknown parametrized family of chaotic dynamical systems from a variety of its time series data with a change in the bifurcation parameters. In an experimental situation, in which no *a priori* analytical knowledge of the dynamical systems is available, we present an algorithm for estimating the underlying bifurcation parameters of the chaotic time series. First, we construct a “qualitatively similar” parametrized family of nonlinear predictors from the sets of chaotic time series. These chaotic time series are then characterized in terms of the “qualitatively similar” bifurcation parameters of the nonlinear predictors. Numerical experiments using the Rössler equations show the efficiency of the algorithm.

25.1 Introduction

Suppose we have an unknown system, A , whose dynamical state is recorded into a single time series $\{\xi_t\}$. Time series analysis in general aims to study the dynamical structure of the underlying system A , using only the time series $\{\xi_t\}$. Since we focus on chaotic dynamics, our particular interest is in detecting the *deterministic nonlinear low-dimensional chaotic property* of the time series.

To date, many algorithms have been developed to characterize the chaotic property of the time series [1, 2]. These algorithms estimate the statistical properties of the underlying chaotic attractors, such as fractal dimension [3], Lyapunov spectrum [4–6], and Kolomogorov-Sinai entropy [7].

Although the conventional studies mainly deal with chaotic time series generated from a single dynamical system, in this chapter we attempt to analyze more detailed dynamical structures such as the bifurcation structure that underlies the chaotic time series.

For this purpose, we consider the following problem (see Fig. 25.1):

“There exists an unknown system, A , whose dynamics is changed by a set of external conditions, namely, bifurcation parameters $p = (p_1, \dots, p_m)$. From such a system A , we record I sets of chaotic time series $\{\xi_t(p(i))\}_{i=1, \dots, I}$ associated with different bifurcation parameter values $\{p(i)\}_{i=1, \dots, I}$. Here, assume that we have no knowledge of the system A , such as the functional form of the dynamics, its dependence on the bifurcation parameters, and the bifurcation parameter values $\{p(i)\}_{i=1, \dots, I}$.”

There exist many practical examples for this problem formulation. In chemical or physical experiment, it is in general impossible to reproduce exactly the same experimental settings in the daily recording. Every recording data therefore should be different from the others, because there should be some changes in the daily experimental conditions. Another example is a chaotic chemical sensor, which is designed to evaluate the taste of food by using a membrane oscillator put in a chemical liquid [8]. With a change in the proportion of the chemical ingredients, the sensory membrane system exhibits a variety of complex oscillatory patterns such as chaos.

Given a set of time series, $\{\xi_t(p(i))\}_{i=1, \dots, I}$, associated with different bifurcation parameter values, we consider a most efficient way to characterize the time series.

In conventional chaotic time series analysis, statistical quantities such as the fractal dimension and the Lyapunov spectrum are used for characterization. This approach, however, has severe limitations. Suppose, for example, we try to distinguish the difference between two time series. If the bifurcation parameter values, undergoing within the two time series, are close to each other, then the statistical properties of the two time series will be similar to each other. Hence,

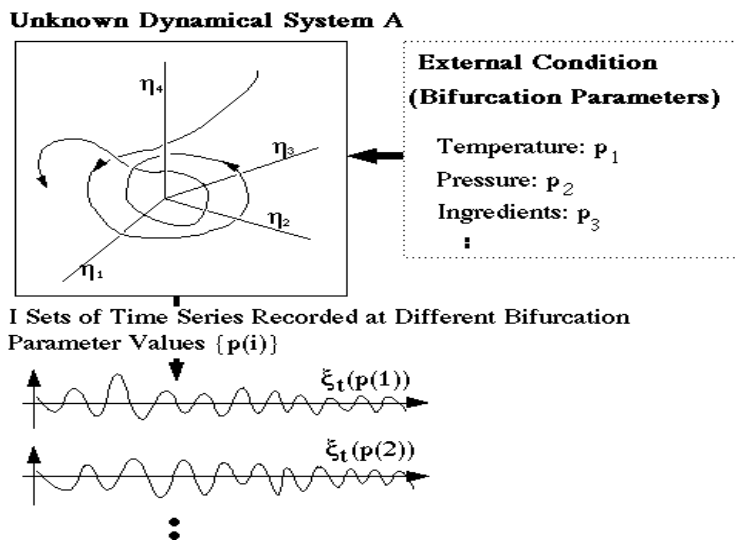


FIGURE 25.1

Problem setting: There exists an unknown dynamical system, A , which exhibits a variety of oscillatory patterns with a change in its external conditions, i.e., the bifurcation parameters $p = (p_1, \dots, p_m)$. At different bifurcation parameter values $\{p(i)\}_{i=1, \dots, I}$, I sets of chaotic time series $\{\xi_t(p(i))\}_{i=1, \dots, I}$ are recorded from the system A .

detection of a slight difference between the two time series by estimating their statistical quantities might be quite difficult.

Since the dynamical structure of the time series is changed by the bifurcation parameters, it is natural to characterize the time series $\{\xi_t(p)\}$ in terms of the associated bifurcation parameter values p . In order to distinguish our standpoint from the conventional one, we call the characterization of chaotic time series in terms of the underlying bifurcation parameters, “recognition” of chaotic time series.

In order to “recognize” chaotic time series, it is necessary to estimate the underlying bifurcation parameter values from time series. Since the problem provides no information about the bifurcation parameters and their family of dynamics, estimation of the exact bifurcation parameter values is practically impossible. However, it is possible to estimate “qualitatively similar” bifurcation parameter values instead. Here, “qualitatively similar” bifurcation parameters mean that the parameters give rise to a family of dynamical systems that exhibit bifurcation phenomena qualitatively similar to those of the original family.

In the investigation of nonlinear predictions [9–13], several interesting studies have been carried out for reconstructing a qualitatively similar parametrized family of chaotic dynamics using a parametrized family of nonlinear predictors. In [9], although no specific results are presented, some schemes for reconstructing a parametrized family of chaotic dynamics using nonlinear predictors have been discussed. In [12], some experimental results on reconstructing a one-parameter family of discrete-time dynamical systems have been reported, based on the assumption that the sets of bifurcation parameter values and the associated time series are known and are available.

Our approach to the problem is based on a simple algorithm proposed in [14, 15]. The algorithm attempts to reconstruct a family of dynamical systems from time series under the condition that the underlying bifurcation parameter values are unknown. The efficiency of the algorithm is shown by reconstructing three families of dynamical systems: the Hénon family, the coupled logistic/delayed-logistic family, and the Rössler family.

In this chapter, we review the algorithm developed in [14, 15] and demonstrate its applicability to the problem of “recognizing” chaotic time series.

This chapter is organized as follows. In Sec. 25.2, an algorithm for reconstructing a parametrized family of chaotic dynamics is first described. In Sec. 25.3, the algorithm is tested against the Rössler family with two parameters. In Sec. 25.4, experimental study is reported for “recognizing” chaotic time series. Finally, Sec. 25.5 is devoted to some discussions with conclusions.

25.2 Reconstructing a Parametrized Family of Chaotic Dynamics

Consider a parametrized family of continuous-time dynamical systems:

$$\frac{d\eta_t}{dt} = f(p, \eta_t), \quad \eta_t \in \mathbf{R}^D, \quad p \in \mathbf{R}^m, \quad (25.2.1)$$

and their observations:

$$\{\xi_t(p) = g(\eta_t(p)) : 0 \leq t \leq T\}, \quad (25.2.2)$$

at I different sets of parameter values:

$$p \in \{p(i)\}_{i=1,2,\dots,I}, \quad (25.2.3)$$

where $g : \mathbf{R}^n \rightarrow \mathbf{R}^1$ is a smooth observation function and $\eta_t(p)$ is a solution for (25.2.1) at the parameter values p . Here, we assume the followings:

- (1) The functional form of the parametrized family of vector fields $f : \mathbf{R}^m \times \mathbf{R}^D \rightarrow \mathbf{R}^D$ is unknown, but f is assumed to be smooth.

- (2) The functional form of g is unknown, but g is assumed to be smooth.
- (3) $m = \dim p$ and the sets of parameter values $\{p(i)\}_{i=1, \dots, I}$ are unknown, but $\{p(i)\}_{i=1, \dots, I}$ are assumed to be closely located in the parameter space.
- (4) $D = \dim \eta_t$ is unknown.
- (5) I sets of time series, $\{\xi_t(p(i))\}_{i=1, \dots, I}$, are all chaotic.

Under conditions (1)–(5), we reconstruct an unknown parametrized family of dynamical systems from the available time series.

The algorithm is mainly composed of two steps: First, within a same parametrized family, nonlinear predictors $F(\Omega, \cdot)$, which model I sets of time series $\{\xi_t(p(i))\}_{i=1, \dots, I}$, are constructed. This means that I sets of nonlinear prediction parameters $\{\Omega(p(i))\}_{i=1, \dots, I}$, which correspond to each time series $\{\xi_t(p(i))\}_{i=1, \dots, I}$, are sought. Second, by the singular value decomposition, principal components Γ are extracted from the nonlinear prediction parameters $\{\Omega(p(i))\}_{i=1, \dots, I}$.

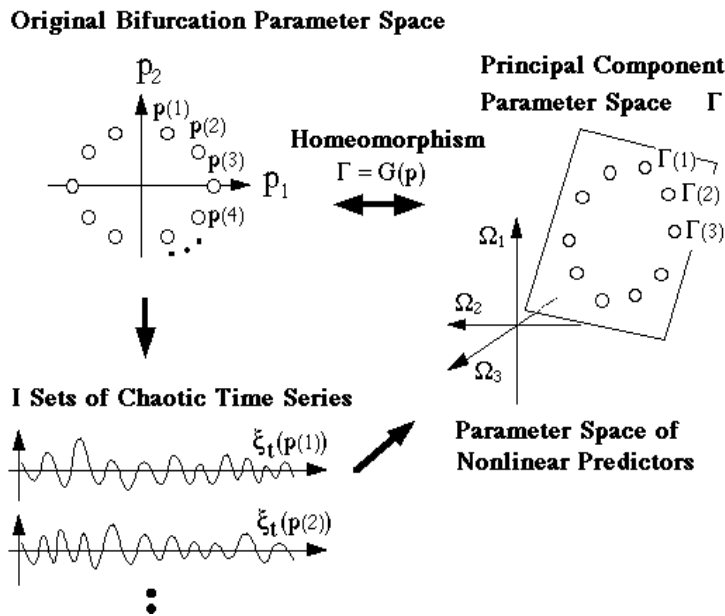


FIGURE 25.2

Basic algorithm: Within a same parametrized family, nonlinear predictors $F(\Omega, \cdot)$ are constructed for chaotic time series $\{\xi_t(p(i))\}_{i=1, \dots, I}$. Then, principal components Γ are extracted from the nonlinear prediction parameters Ω . If there exists a one-to-one correspondence between Γ and p , the principal parameters Γ are considered as the “qualitative” parameters of the original bifurcation parameters p .

As illustrated in Fig. 25.2, in the principal component parameter space Γ , we define a parametrized family of nonlinear predictors $F(\Gamma, \cdot)$.

As is shown by the following numerical experiments, the principal component parameters Γ can be considered as the “qualitative” parameters of the original bifurcation parameters p , in the sense that: (1) There seems to exist a one-to-one correspondence between Γ and p ; (2) The parametrized family $F(\Gamma, \cdot)$ gives rise to qualitatively similar bifurcation phenomena as the original $f(p, \cdot)$.

25.2.1 Average filtering of chaotic time series

Since time series are usually sampled digitally in laboratory experiments, let (25.2.2) be rewritten as

$$\{\xi_n(p) = g(\eta_{n\Delta t}(p)) : n = 1, \dots, N\}, \quad (25.2.4)$$

where $\eta_t(p)$ is a solution for (25.2.1) at the parameter values p , and Δt is a sampling rate.

In order to reduce the noise effect, an averaging filter is applied to the time series of (25.2.4). The filtered time series are given by

$$\{\hat{\xi}_n(p(i)) = \frac{\sum_{k=n}^{n+W} \xi_k(p(i))}{W\Xi} : n = 1, \dots, N - W\}_{i=1, \dots, I}, \quad (25.2.5)$$

$$\text{with } \Xi = \max_{n,i} \left(\left| \sum_{k=n}^{n+W} \xi_k(p(i)) \right| \right), \quad (25.2.6)$$

where $W + 1$ is the window length of the moving average and Ξ is a normalization constant.

25.2.2 Nonlinear predictors

From the filtered time series $\{\hat{\xi}_n(p(i)) : n = 1, \dots, N - W\}_{i=1, \dots, I}$, a d -dimensional trajectory $\{X_n(p(i)) : n = (d - 1)\tau + 1, \dots, N - W\}_{i=1, \dots, I}$ is reconstructed by using a delay-coordinate [16, 17]:

$$\begin{aligned} X_n(p) &= {}^t(x_n(p), {}^2x_n(p), \dots, {}^dx_n(p)) \\ &= {}^t(\hat{\xi}_n(p), \hat{\xi}_{n-\tau}(p), \hat{\xi}_{n-2\tau}(p), \dots, \hat{\xi}_{n-(d-1)\tau}(p)), \end{aligned} \quad (25.2.7)$$

where t denotes transposition. The Filtered Delay Embedding Prevalence Theorem [17] guarantees that the reconstructed trajectory $\{X_n(p(i))\}_{i=1, \dots, I}$ is qualitatively the same as the original $\{\eta_{n\Delta t}(p(i))\}_{i=1, \dots, I}$.

Next, for each reconstructed trajectory, $\{X_n(p(i))\}_{i=1, \dots, I}$, we seek an ordinary differential equation of the form

$$\frac{d\phi^t}{dt} = F(\Omega, \phi^t), \quad (25.2.8)$$

that satisfies

$$X_{n+k}(p(i)) = \phi^{k\Delta t}(\Omega(p(i)), X_n(p(i))) \quad (25.2.9)$$

for $k = 1, \dots, K$,

where $\Omega \subset \mathbf{R}^L$ stands for a set of parameters of nonlinear function $F(\cdot, \cdot)$, $\phi^t : \mathbf{R}^L \times \mathbf{R}^d \rightarrow \mathbf{R}^d$ stands for a solution of (25.2.8) at $\Omega = \Omega(p(i))$ with an initial condition $\phi^0(\Omega, X) = X$, and K stands for the maximum time steps, where L will be specified later.

As the nonlinear function model $F : \mathbf{R}^L \times \mathbf{R}^d \rightarrow \mathbf{R}^d$, the multi-layer perceptron (MLP) [18–21] is exploited in this chapter, where the MLP composed of three-layers (d -units in the input layer, h -units in the hidden layer, and d -units in the output layer) is given by

$$F(\Omega, \phi) = {}^t(F_1(\Omega, \phi), F_2(\Omega, \phi), \dots, F_d(\Omega, \phi)), \quad (25.2.10)$$

where

$$F_k(\Omega, \phi) = \sum_{j=1}^h \omega_{(k-1)h+j} \sigma \left(\sum_{i=1}^d \omega_{dh+(j-1)d+i} {}^i\phi + \omega_{2dh+j} \right) \quad (k = 1, \dots, d),$$

$$\sigma(x) = \frac{2.0}{1 + e^{-x}} - 1.0,$$

$$\Omega = {}^t(\omega_1, \omega_2, \dots, \omega_L) \quad \text{with } L = (2d + 1)h,$$

$$\phi = {}^t({}^1\phi, {}^2\phi, \dots, {}^d\phi).$$

The parameters $\{\Omega(p(i))\}_{i=1, \dots, I}$ of the nonlinear function F , which models the data dynamics $\{X_n(p(i))\}_{i=1, \dots, I}$, are computed in the following manner: First, the reconstructed data are periodically ordered as

$$\{X_n(p(1))\}, \{X_n(p(2))\}, \dots, \{X_n(p(I))\}, \\ \{X_n(p(I+1))\} (= \{X_n(p(1))\}), \dots \quad (25.2.11)$$

Second, $\Omega(p(1))$, which minimizes the cost function:

$$U(\Omega) = \sum_{n=(d-1)\tau+1}^{N-W-K} \sum_{k=1}^K \frac{1}{2} |X_{n+k}(p(1)) - \phi^{k\Delta t}(\Omega, X_n(p(1)))|^2, \quad (25.2.12)$$

are computed via the quasi-Newton method¹ [22], where the initial condition for

¹In the quasi-Newton method, a local minimum of the cost function (25.2.12) is sought by the iterative procedure of $\Omega_{n+1} = \Omega_n - H_n \nabla U(\Omega_n)$, where $\nabla U(\Omega_n)$ and H_n stand for a gradient vector and an approximation of the inverse Hessian of $U(\Omega)$ at $\Omega = \Omega_n$. There is a variety of update formulas for estimating a series of $\{H_n\}$. In our numerical experiments, we exploit the Broyden-Fletcher-Goldfarb-Shanno formula with Luenberger's self-scaling formula.

$\Omega(p(1))$ is given by a set of random values, uniformly distributed over $[0, 0.1]^L$.

In a similar manner, $\Omega(p(i))$ ($2 \leq i$) are computed by minimizing the cost function (25.2.12) defined for the reconstructed data $\{X_n(p(i))\}$, where $\Omega(p(i-1))$ are used as the initial condition instead of random values.

In our numerical experiments, we set the number of the quasi-Newton's iteration steps to 20 for $i < 10I$ and 40 for $10I \leq i$.

The procedures for computing $\{\Omega(p(i))\}_{i=1,2,\dots}$ are repeated until they converge to a periodic sequence, as

$$\begin{aligned} \Omega(p(N_I)), \Omega(p(N_I + 1)), \dots, \Omega(p(N_I + I)), \\ \Omega(p(N_I + I + 1)) (= \Omega(p(N_I))), \dots, \end{aligned} \quad (25.2.13)$$

where N_I is assumed to be sufficiently large.

25.2.3 Extracting principal bifurcation parameters

In the final step of the algorithm, principal component parameters are extracted from the L -dimensional parameters of Ω , by the Karhunen-Loève (KL) transform [23–26].

First, we consider the subsequence of the parameters $\{\Omega(p(i)) : i = N_I, N_I + 1, \dots, N_I + N_J - 1\}$, and compute $\{\delta\Omega_i : i = 1, \dots, N_J\}$ and Ω_0 , as

$$\Omega_0 = \frac{1}{N_J} \sum_{i=1}^{N_J} \Omega(p(N_I + i - 1)), \quad (25.2.14)$$

$$\delta\Omega_i = \Omega(p(N_I + i - 1)) - \Omega_0, \quad (25.2.15)$$

where N_J stands for the number of the elements.

Second, the multivariate distribution of $\{\delta\Omega_i : i = 1, \dots, N_J\}$ is computed in terms of the covariance matrix:

$$\Omega_{L \times L} = \frac{1}{N_J} \sum_{i=1}^{N_J} \delta\Omega_i \ ^t\delta\Omega_i. \quad (25.2.16)$$

Since $\Omega_{L \times L}$ has non-negative eigenvalues $\{\lambda_1, \lambda_2, \dots, \lambda_L\}$, we arrange them in descending order, as

$$\lambda_1 \geq \lambda_2 \geq \dots \geq \lambda_L \geq 0. \quad (25.2.17)$$

Applying the KL-transformation to $\delta\Omega$, the principal parameters are obtained as

$$\Gamma = (\gamma_1, \gamma_2, \dots, \gamma_L) = \ ^t[u_1 | u_2 | \dots | u_L]^{-1} \delta\Omega \quad (25.2.18)$$

where $\{u_1, u_2, \dots, u_L\}$ stand for the eigenvectors corresponding to $\{\lambda_1, \lambda_2, \dots, \lambda_L\}$.

Since transformation (25.2.18) diagonalizes the covariance matrix (25.2.16) in the Γ -space, the diagonal elements $\{\lambda_1, \lambda_2, \dots, \lambda_L\}$ represent significance of their corresponding principal parameters $\{\gamma_1, \gamma_2, \dots, \gamma_L\}$.

Finally, by computing the normalized eigenvalues

$$\Lambda_i = 100 \times \frac{\lambda_i}{\sum_{j=1}^L \lambda_j} [\%] \quad (i = 1, \dots, L), \quad (25.2.19)$$

the number of significant parameters M is determined. If the nonlinear prediction parameters $\{\delta\Omega_i : i = 1, \dots, N_J\}$ are all confined in the m -dimensional linear subspace of $\delta\Omega$, we can expect that $M = m$ and that $\Gamma_m = {}^t(\gamma_1, \gamma_2, \dots, \gamma_m)$ represents the significant set of parameters for the nonlinear predictors (25.2.8).

With respect to the significant parameters Γ_m , the m -parameter family of nonlinear predictors is given by

$$\frac{d\phi^t}{dt} = F(\Omega(\Gamma_m), \phi^t), \quad (25.2.20)$$

where

$$\Omega(\Gamma_m) = {}^t[u_1 \mid u_2 \mid \dots \mid u_L]^{-1}[\Gamma_m \mid 0] + \Omega_0, \quad (25.2.21)$$

where 0 denotes an $(L - m)$ -dimensional zero column vector.

Since the sequence of the significant parameters

$$\Gamma_m(p(1)) \rightarrow \Gamma_m(p(2)) \rightarrow \dots \rightarrow \Gamma_m(p(N_J)) \quad (25.2.22)$$

can be considered as the image of the sequence of the original bifurcation parameters

$$p(1) \rightarrow p(2) \rightarrow \dots \rightarrow p(I) \rightarrow p(I+1)(=p(1)) \rightarrow \dots \quad (25.2.23)$$

in the significant parameter space of nonlinear predictors, we call the original sequence of (25.2.23) “bifurcation path” and its corresponding sequence of (25.2.22) “bifurcation locus.”

25.3 Numerical Experiment on the Rössler Equations

Now, we test the algorithm against the Rössler equations [27]:

$$\begin{aligned}\frac{d^1 \eta_t}{dt} &= {}^2 \eta_t - {}^3 \eta_t, \\ \frac{d^2 \eta_t}{dt} &= {}^1 \eta_t - p_2 {}^2 \eta_t, \\ \frac{d^3 \eta_t}{dt} &= p_3 {}^1 \eta_t - p_1 {}^3 \eta_t + {}^1 \eta_t {}^3 \eta_t.\end{aligned}\tag{25.3.24}$$

We selected the Rössler equations as the testing example for two reasons: The bifurcation structure of the equations has been well studied (e.g., [28]) and this bifurcation structure is fairly moderate.

In this experiment, p_3 is fixed as

$$p_3 = 0.3,\tag{25.3.25}$$

so that the system (25.3.24) is considered as a two-parameter family. Figure 25.3 (a) shows a local bifurcation diagram of (25.3.24), with

$$(p_1, p_2) \in [4.3, 5.7] \times [0.30, 0.36],\tag{25.3.26}$$

while Fig. 25.3 (b) shows a global bifurcation diagram, with

$$(p_1, p_2) \in [3.814, 8.814] \times [0.25, 0.429].\tag{25.3.27}$$

The bifurcation diagram shows the existence domain of periodic attractors, where the color indicates the number of their periods (see the colored samples in Fig. 25.3 (e)).

The bifurcation structures shown in Figs. 25.3 (a) and (b) have been thoroughly studied by Gaspard-Kapral-Nicolis [28]. On the (p_1, p_2) -parameter space, it is clearly seen that “fishhook”-like periodic windows form a spiral structure. In the upper-half region of Fig. 25.3 (b), (25.3.24) has a homoclinic orbit, which passes through the origin and generates a “screw”-type strange attractor. In the lower-half region, on the other hand, (25.3.24) has no homoclinic orbit with respect to the origin and exhibits a “spiral”-type strange attractor.

25.3.1 Reconstructing bifurcation diagrams

Consider twelve different sets of parameter values (see Fig. 25.4 (a)):

$$\begin{aligned}p(i) &= (p_1(i), p_2(i)) \\ &= \left(0.7 \sin\left(2\pi \frac{(i-1)}{12}\right) + 5.0, 0.03 \cos\left(2\pi \frac{(i-1)}{12}\right) + 0.33 \right)\end{aligned}\tag{25.3.28}$$

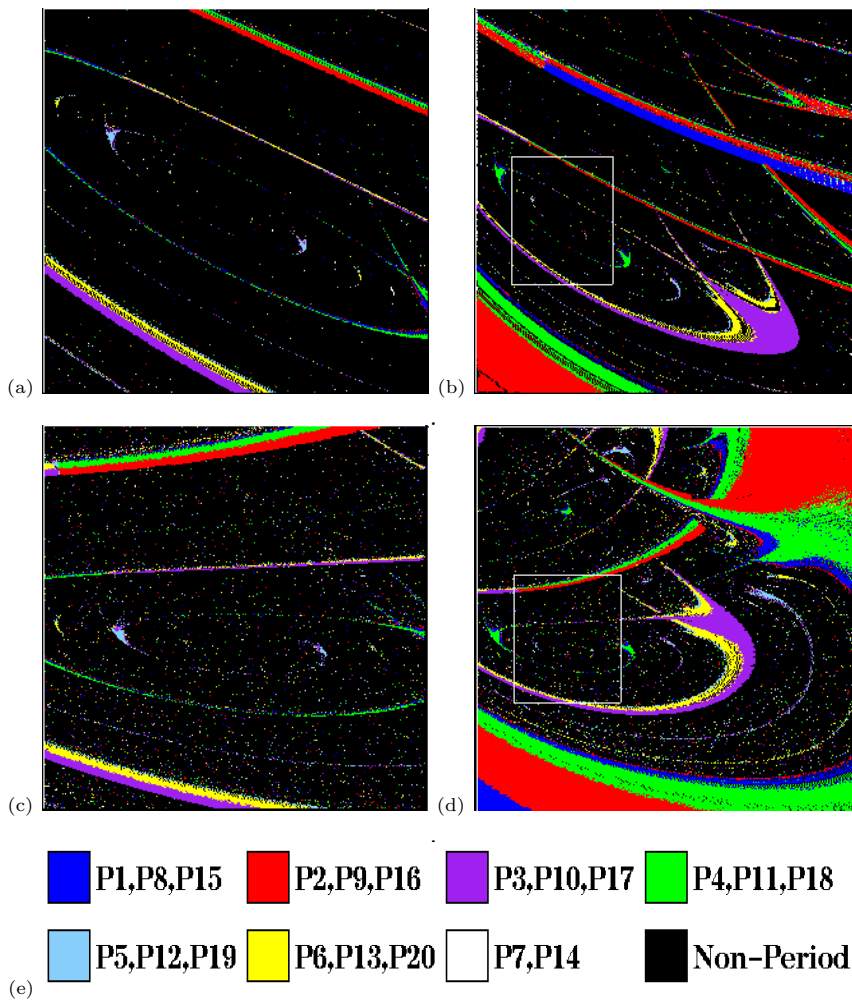


FIGURE 25.3
 (a) (p_1, p_2) -bifurcation diagram of the Rössler equations with $(p_1, p_2) \in [4.3, 5.7] \times [0.30, 0.36]$. (b) (p_1, p_2) -bifurcation diagram of the Rössler equations with $(p_1, p_2) \in [3.814, 8.814] \times [0.25, 0.429]$. The rectangle region corresponds to the bifurcation diagram of Fig. 25.3 (a). (c) (γ_1, γ_2) -bifurcation diagram of the nonlinear predictors (25.2.20) with $(\gamma_1, \gamma_2) \in [-0.103, 0.105] \times [-0.044, 0.051]$. (d) $(\gamma_1, -\gamma_2)$ -bifurcation diagram of the nonlinear predictors (25.2.20) with $(\gamma_1, \gamma_2) \in [-0.175, 0.568] \times [-0.123, 0.160]$. The rectangle region corresponds to the bifurcation diagram of Fig. 25.3 (c). (e) The colored samples.

and measure the associated time series

$$\{\xi_n(p(i)) = {}^2\eta_{\kappa+n\Delta t}(p(i)) : n = 1, \dots, 3000\}_{i=1, \dots, 12}, \quad (25.3.29)$$

where each trajectory is calculated by numerically integrating (25.3.24) with initial condition $\eta_0 = {}^t(0.05, 0, 0)$ by using the fourth-order Runge-Kutta algorithm with a time step of 0.01. The transient time and the sampling rate are set to $(\kappa, \Delta t) = (2.0, 0.2)$.

Following the procedures described in Sec. 25.2, we first reconstruct trajectories $\{X_n(p(i))\}_{i=1, \dots, 12}$ in a filtered delay-coordinate space with $(d, W, \tau) = (3, 8, 4)$. Here, the reconstruction dimension d is set equal to the dimension of the original dynamical system, since one can estimate the dimension by a variety of time series analyses, e.g., [3, 24]. Of course, our procedure works well for d larger than three.

Second, using the nonlinear predictors defined by (25.2.8) with $h = 10$, we seek the parameters $\{\Omega(p(1)), \Omega(p(2)), \dots\}$ corresponding to

$$\begin{aligned} &\{X_n(p(1))\}, \{X_n(p(2))\}, \dots, \{X_n(p(12))\}, \\ &\{X_n(p(13))\} (= \{X_n(p(1))\}), \dots \end{aligned} \quad (25.3.30)$$

by minimizing the cost function defined by (25.2.12) with $K = 4$.

Finally, we extract principal component parameters $\{\gamma_1, \gamma_2, \dots\}$ of Ω by applying the KL-transform to subsequence

$$\begin{aligned} &\{\Omega(p(N_I)), \Omega(p(N_I + 1)), \dots, \Omega(p(N_I + N_J - 1))\} \quad (25.3.31) \\ &\text{with } (N_I, N_J) = (1440, 24). \end{aligned}$$

The solid line of Fig. 25.4 (b) shows the normalized eigenvalues $\{\Gamma_k = 100 \times \lambda_k / \sum_{j=1}^{70} \lambda_j [\%] : k = 1, \dots, 10\}$ of the covariance matrix (25.2.16) and the broken line shows their accumulated sums $\{\sum_{j=1}^k \Gamma_j [\%] : k = 1, \dots, 10\}$. Since Fig. 25.4 (b) shows that $\sum_{j=1}^2 \Gamma_j > 95[\%]$, it is clearly seen that the principal component parameters of (25.3.31) are $\Gamma_2 = (\gamma_1, \gamma_2)$. The dimension of the bifurcation parameters p is therefore correctly estimated as $m = 2$.

Figure 25.4 (c) shows the bifurcation locus in the (γ_1, γ_2) -space. Compared to the bifurcation path of Fig. 25.4 (a), the original configuration of the bifurcation path is preserved in the bifurcation locus without any large distortion.

Correspondence between the principal parameters and the original ones can be roughly illustrated as $p_1 \leftrightarrow \gamma_1$ and $p_2 \leftrightarrow \gamma_2$.

Figures 25.3 (c) and (d) show bifurcation diagrams of the reconstructed family of dynamical systems (25.2.20) in the (γ_1, γ_2) -space. The local bifurcation diagram of Fig. 25.3 (c) reproduces qualitatively similar bifurcation phenomena as the original. The bifurcation structures with continually connected fishhooks are discernible.

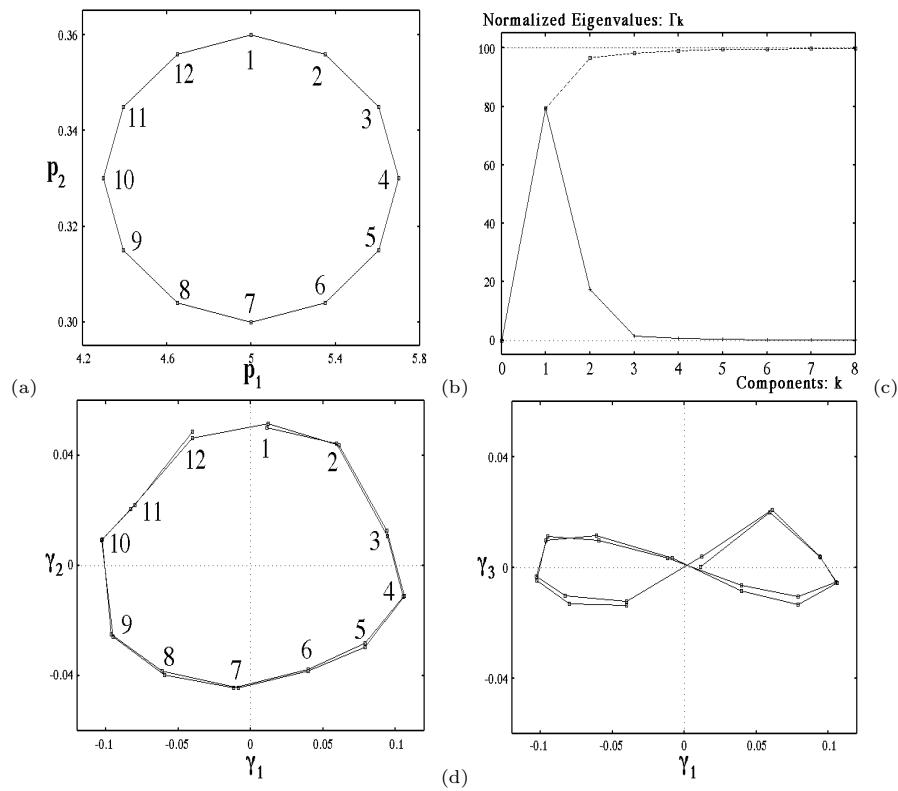


FIGURE 25.4

(a) Bifurcation path in the (p_1, p_2) -space. (b) Normalized eigenvalues $\{\Gamma_k = 100 \times \lambda_k / \sum_{j=1}^{70} \lambda_j [\%] : k = 1, \dots, 10\}$ (solid line) of the principal components and their accumulated sums $\{\sum_{j=1}^k \Gamma_j [\%] : k = 1, \dots, 10\}$ (broken line). (c) Bifurcation locus in the (γ_1, γ_2) -space. (d) Bifurcation locus in the (γ_1, γ_3) -space.

In Fig. 25.4 (d), bifurcation locus in the (γ_1, γ_3) -space is shown. We see that the amplitude of γ_3 eventually increases for large $|\gamma_1|$. This indicates that the image of the original parameter space p on the Γ -space is not exactly confined in the (γ_1, γ_2) -space. The approximation error due to describing the distorted image by a two-dimensional linear surface may grow in the outer region. This might be the original cause of the bifurcation structures being qualitatively different from the original ones discernible in the outer region of the global bifurcation diagram of Fig. 25.3 (d). The situation might be improved by approximating the nonlinear manifold by nonlinear transformations.

25.4 Recognizing Chaotic Time Series

In this section, we apply the qualitative family of nonlinear predictors constructed in Sec. 25.3 for the “recognition” of chaotic time series. Here, we characterize chaotic time series $\{\xi_n(p^*)\}$ by estimating its associated bifurcation parameter values p^* in terms of its image in the nonlinear prediction parameter space $\Gamma_2(p^*)$.

For chaotic time series:

$$\{\xi_n(p^*) = \eta_{\kappa+n\Delta t}(p^*) : n = 1, \dots, 3000\}, \quad (25.4.32)$$

recorded in the same condition as (25.3.29), the corresponding bifurcation parameters $\Gamma_2(p^*)$ are sought by minimizing the cost function:

$$U(\Gamma_2) = \sum_{n=(d-1)\tau+1}^{N-W-K} \sum_{k=1}^K \frac{1}{2} |X_{n+k}(p^*) - \phi^{k\Delta}(\Gamma_2, X_n(p^*))|^2 \quad (25.4.33)$$

where $\phi^t : \mathbf{R}^2 \times \mathbf{R}^d \rightarrow \mathbf{R}^d$ stands for a solution of (25.2.20) at the parameter values Γ_2 with an initial condition $\phi^0(\Gamma_2, X) = X$.

For 48 sets of bifurcation parameter values (see Fig. 25.5 (a)):

$$\begin{aligned} p(i) &= (p_1(i), p_2(i)) \\ &= \left(R_1 \cos\left(2\pi \frac{(i-1)}{12}\right) + 5.0, R_2 \sin\left(2\pi \frac{(i-1)}{12}\right) + 0.33 \right) \\ &\quad (i = 1, \dots, 12) \end{aligned}$$

$$\text{with } (R_1, R_2) = (0.35, 0.015), (0.7, 0.03), (1.4, 0.06), (2.1, 0.09), \quad (25.4.34)$$

the corresponding parameters $\{\Gamma_2(p(i))\}$ in the Γ_2 -space are estimated.

Figure 25.5 (b) shows the results of the “recognition” of chaotic time series. From the similar configurations discernible in the locations of the corresponding

bifurcation parameters in the p -space and the Γ_2 -space, we see that parameters qualitatively similar to the original p can be estimated in the Γ_2 -space. This implies that there exists a one-to-one correspondence between the original bifurcation parameters p and the nonlinear prediction parameters Γ_2 .

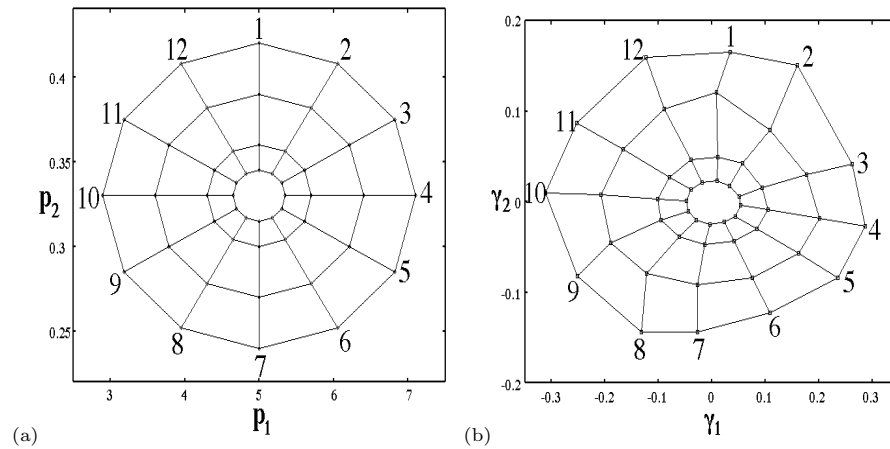


FIGURE 25.5 Experiment for recognizing chaotic time series. (a) Selected parameters in the (p_1, p_2) -space. (b) Estimated parameters in the (γ_1, γ_2) -space.

25.5 Discussions and Conclusions

In this chapter, a method has been described for constructing a parametrized family of nonlinear predictors “qualitatively similar” to a family of chaotic dynamics. Numerical experiments using the Rössler equations have demonstrated the efficiency of the algorithm.

On the basis of the family qualitatively similar to the Rössler equations, it was shown that chaotic time series can be systematically characterized in terms of the qualitative parameters of the nonlinear predictors. Our experiments therefore demonstrated the applicability of the method for “recognizing” chaotic time series.

In the present experiment, robustness of the algorithm against noise was not considered. For a moderate amount of observational noise, we have confirmed that the algorithm works efficiently [15]. It is, however, necessary to consider limitations of the algorithm against very large observational noise and dynamical noise.

In nonlinear time series analysis of complex real-world data, the following question often arises:

Does the irregularity observed in real-world time series originate from deterministic chaos or stochastic dynamics?

The conventional approach to answering the above question has been attempting to characterize chaos by analysing a single set of time series data [1, 2]. This type of approach can sometimes be controversial, because accurate characterization of chaotic properties becomes very difficult when time series data are very short and when time series data are contaminated with strong noise.

We emphasize that our approach of identifying a parametrized family of chaotic dynamics from time series can potentially solve this problem. If a low-dimensional bifurcation structure is clearly detected by our algorithm, then, our algorithm gives the strongest evidence for low-dimensional chaos in real-world time series, because stochastic dynamics can never give rise to such smooth low-dimensional bifurcations. As a method to detect chaos with the strongest evidence, our algorithm will be further applied to a variety of real-world time series data.

Finally, we note that the algorithm described in this chapter has recently been extended to analysis of non-stationary time series and to synchronization analysis of coupled nonlinear oscillators. Interested readers are referred to [29] and [30] for details.

References

- [1] H. D. I. Abarbanel, R. Brown, J. J. Sidorowich, and L. S. Tsimring, "The analysis of observed chaotic data in physical systems," *Rev. Mod. Phys.*, Vol. 65, pp. 1331-1392, 1993.
- [2] H. Kantz and T. Schreiber, *Nonlinear Time Series Analysis*, Cambridge University Press, Cambridge UK, 1997.
- [3] P. Grassberger and I. Procaccia, "Measuring the strangeness of strange attractors," *Physica D*, Vol. 9, pp. 189-208, 1983.
- [4] M. Sano and Y. Sawada, "Measurement of the Lyapunov spectrum from chaotic time series," *Phys. Rev. Lett.*, Vol. 55, pp. 1082-1085, 1985.
- [5] A. Wolf, J. B. Swift, H. L. Swinney, and J. A. Vastano, "Determining Lyapunov exponents from a time series," *Physica D*, Vol. 16, pp. 285-317, 1985.
- [6] J. P. Eckmann, S. O. Kanmphorst, D. Ruelle, and S. Ciliberto, "Liapunov exponents from a time series," *Phys. Rev. A*, Vol. 34, pp. 4971-4979, 1986.
- [7] A. M. Fraser, "Information and entropy in strange attractors," *IEEE Trans. Info. Theory*, Vol. 35, pp. 245-262, 1989.
- [8] Y. Saida, T. Matsuno, and K. Yamafuji, *Sensors and Materials*, Vol. 4, p. 135, 1992.
- [9] J. P. Crutchfield and B. S. McNamara, "Equations of motion from a data series," *Complex Systems*, Vol. 1, pp. 417-452, 1987.
- [10] J. D. Farmer and J. J. Sidorowich, "Predicting chaotic time series," *Phys. Rev. Lett.*, Vol. 59, pp. 845-848, 1987.
- [11] A. Lapedes and R. Farber, "Nonlinear signal processing using neural networks: Prediction and system modeling," *Tech. Rep. Los Alamos Nat. Lab.*, LA-UR-87-2662, 1987.
- [12] M. Casdagli, "Nonlinear prediction of chaotic time series," *Physica D*, Vol. 35, pp. 335-356, 1989.
- [13] G. Sugihara and R.M. May, "Nonlinear forecasting as a way of distinguishing chaos from measurement error in time series," *Nature*, Vol. 344, pp. 734-741, 1990.
- [14] R. Tokunaga, S. Kajiwara, and T. Matsumoto, "Reconstructing bifurcation diagrams only from time waveforms," *Physica D*, Vol. 79, pp. 348-360, 1994.
- [15] I. Tokuda, S. Kajiwara, R. Tokunaga, and T. Matsumoto, "Recognizing chaotic time-waveforms in terms of a parametrized family of nonlinear predictors," *Physica D*, Vol. 95, pp. 380-395, 1996.
- [16] F. Takens, "Detecting strange attractors in turbulence," in *Lecture Notes in Math.*, Vol. 898, Springer, Berlin, pp. 366-381, 1981.
- [17] T. Sauer, J. A. York, and M. Casdagli, "Embedology," *J. Stat. Phys.*, Vol. 65, pp. 579-616, 1991.

- [18] D. E. Rumelhart, J. L. McClelland, and the PDP Research Group, *Parallel Distributed Processing*, MIT Press, Cambridge, 1986.
- [19] G. Cybenko, "Approximation by superpositions of a sigmoidal function," *Math. Control Signals Systems*, Vol. 2, pp. 303-314, 1989.
- [20] K. Funahashi, "On the approximate realization of continuous mappings by neural networks," *Neural Networks*, Vol. 2, pp. 183-192, 1989.
- [21] K. Hornik, "Multilayer feedforward networks are universal approximators," *Neural Networks*, Vol. 2, pp. 359-366, 1989.
- [22] D. G. Luenberger, *Linear and Nonlinear Programming*, Addison-Wesley, 1973.
- [23] T. W. Anderson, *An Introduction to Multivariate Statistical Analysis*, Wiley, 1958.
- [24] D. S. Broomhead and G. P. King, "Extracting qualitative dynamics from experimental data," *Physica D*, Vol. 20, pp. 217-236, 1986.
- [25] A. I. Mees, P. E. Rapp, and L. S. Jennings, "Singular-value decomposition and embedding dimension," *Phys. Rev. A*, Vol. 36, pp. 341-346, 1987.
- [26] A. M. Albano, J. Muench, C. Schwartz, A. I. Mees, and P. E. Rapp, "Singular-value decomposition and the Grassberger-Procaccia algorithm," *Phys. Rev. A*, Vol. 38, pp. 3017-3026, 1988.
- [27] O. E. Rössler, "Continuous chaos," *Ann. New York Acad. Sci.*, Vol. 31, pp. 376-392, 1979.
- [28] P. Gaspard, R. Kapral, and G. Nicolis, "Bifurcation phenomena near homoclinic systems: A two-parameter analysis," *J. Stat. Phys.*, Vol. 35, pp. 697-727, 1986.
- [29] I. Tokuda, R. Tokunaga, and T. Matsumoto, "Detecting switch dynamics in chaotic time-waveform using a parametrized family of nonlinear predictors," *Physica D*, Vol. 135, pp. 63-78, 2000.
- [30] I. Tokuda, J. Kurths, and E. Rosa, Jr., "Learning phase synchronization from nonsynchronized chaotic regimes," *Phys. Rev. Lett.*, Vol. 88, No. 1, 2002, *in press*.

26

Cipher-Quasi-Chaotic Sequence with Application to Spreading Spectrum Communication Systems

Juebang Yu

National Key Lab of Wideband Comm.
Department of Opto-electronic Technology
University of Electronic Science and Technology of China
Chengdu, Sichua 610054
PR China
jbyu@uestc.edu.cn

Abstract

This chapter is devoted to a study of secure chaotic communication, particularly for digital chaotic spreading spectrum communication systems. A schematic of an existing spreading spectrum communication system (SSCS) is shown in Fig. 26.1. In this system, the spreading/dispersing module may work in either DS (direct sequence) or FH (frequency hopping) mode. Our study on chaotic SSCS (CSSCS) is in a broad sense: whenever a chaotic PN (pseudo-noise) sequence (shown by the dotted line in Fig. 26.1) plays a role in any SSCS module (shown by the solid line in Fig. 26.1), it is referred to as a CSSCS.